Electrically Controlled Anomalous Hall Effect and Orbital Magnetization in Topological Magnet $MnBi_2Te_4$

Ruobing Mei,[1] Yi-Fan Zhao,[1] Chong Wang,[2] Yafei Ren,[2] Di Xiao,[2,3] Cui-Zu Chang,[1] and Chao-Xing Liu[1]
[1]*Department of Physics, The Pennsylvania State University, University Park, Pennsylvania 16802, USA*
[2]*Department of Materials Science and Engineering, University of Washington, Seattle, Washington 98195, USA*
[3]*Department of Physics, University of Washington, Seattle, Washington 98195, USA*

(Received 24 April 2023; accepted 22 December 2023; published 9 February 2024)

We propose an intrinsic mechanism to understand the even-odd effect, namely, opposite signs of anomalous Hall resistance and different shapes of hysteresis loops for even and odd septuple layers (SLs), of MBE-grown $MnBi_2Te_4$ thin films with electron doping. The nonzero hysteresis loops in the anomalous Hall effect and magnetic circular dichroism for even-SLs $MnBi_2Te_4$ films originate from two different antiferromagnetic (AFM) configurations with different zeroth Landau level energies of surface states. The complex form of the anomalous Hall hysteresis loop can be understood from two magnetic transitions, a transition between two AFM states followed by a second transition to the ferromagnetic state. Our model also clarifies the relationship and distinction between axion parameter and magnetoelectric coefficient, and shows an even-odd oscillation behavior of magnetoelectric coefficients in $MnBi_2Te_4$ films.

DOI: 10.1103/PhysRevLett.132.066604

Introduction.—The recent discovery of $MnBi_2Te_4$ (MBT) [1–8] provides an excellent platform to explore the interplay between topological physics and magnetism [9,10]. Exotic magnetic topological phases, including the quantum anomalous Hall (QAH) state [11,12], axion insulator (AI) [11–13], and Möbius insulator [14], have been theoretically predicted. For bulk materials, the *A*-type antiferromagnetism, namely, ferromagnetic coupling in one septuple layer (SL) and antiferromagnetic (AFM) coupling between two adjacent SLs, has been unambiguously established through magnetic susceptibility [3,4] and neutron diffraction experiments [2]. Topological Dirac surface states have also been observed in angular-resolved photon emission spectroscopy [3,15–18], although the existence of a magnetic gap is still under debate [4,15,19,20]. These experiments confirmed the coexistence of magnetic order and topological band structure in bulk MBT.

The situation of MBT thin films, however, is subtle. Theoretically, an even-odd effect was predicted for *insulating* MBT films [11–13]. The QAH state can exist for odd SLs while the AI state [11,12,21–37] appears for even SLs. Later experiments combining reflective magnetic circular dichroism (RMCD) and anomalous Hall (AH) measurements, however, challenged this scenario [38–43]. The corresponding hysteresis loops are not synchronized. Specifically, RMCD signals exhibit a clear hysteresis loop for odd SLs whereas the AH hysteresis loop is almost invisible. For even SLs, a small zero-field RMCD signal was reported, whereas a clear AH hysteresis loop was found. These experimental findings indicate the complexity of real materials where the chemical and magnetic environments that depend on individual sample qualities are important.

Recently, another type of even-odd effect was found in *metallic* MBT films grown by molecular beam epitaxy (MBE) [44]. Although the metallic samples with both even and odd SLs show AH hysteresis loops, the loop shapes are clearly distinct. The AH hysteresis loops can be decomposed into two AH components. One behaves the same for even and odd SLs, coming from minor Mn-doped Bi_2Te_3. The other is from the dominant MBT phase, and (i) the signs of zero-field AH resistance are opposite for even and odd SLs; (ii) for even SLs, AH sign reverses twice around spin-flop transition between AFM and canted AFM states in Fig. 1(a), reproducing the measurements in Ref. [44], while no such behavior occurs for odd SLs (Supplemental Material, Sec. I [45]). Similar transport data was also shown in even-SL MBT fabricated by mechanical exfoliation [38,40,53,54]. Given different disorder levels for the samples prepared with different methods, we here explore intrinsic mechanism for this even-odd effect.

In this work, we provide a theoretical understanding of AH hysteresis loops in MBT films based on a two-surface-state model and a four-band thin film model. Our theory suggests that the transition between two nearly degenerate AFM states [Fig. 1(b)] can provide a consistent understanding of both the opposite signs between even and odd SLs and the complex AH hysteresis loop of even SLs in Fig. 1(a). Furthermore, we interpret our results with orbital magnetization [55–58] and extract the magnetoelectric coefficient, which approaches the bulk value determined by the axion parameter as the layer thickness increases for even SLs and stays zero for odd SLs. We clarify the relationship and distinction between axion parameter and magnetoelectric coefficient.

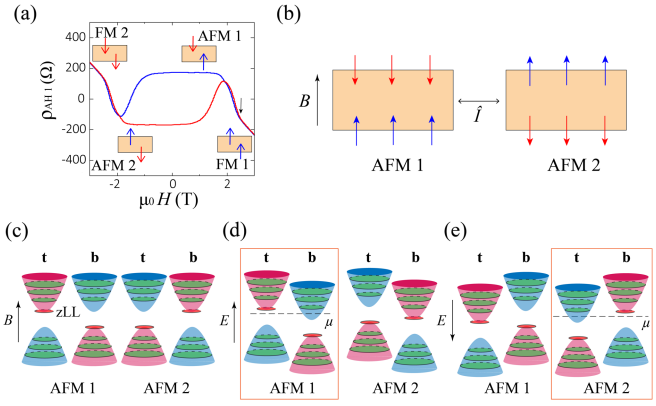

FIG. 1. (a) Experimental measurement of AH resistance ρ_{yx} as a function of magnetic field $\mu_0 H$ in a 2 SL MBT film. The spin-flop field is around 2.3 T, indicated by the black arrow. See Ref. [44] and Supplemental Material Sec. I [45] for more details. The favored AFM states denoted here are for the case with $V_0 > 0$. When $V_0 < 0$, AFM1 and AFM2 are switched. (b) Magnetization configurations of even SL MBT films. (c) Illustration of the two-surface-state model for $g > 0$ and $B > 0$, where "t" and "b" stand for top and bottom surfaces, respectively. Each band is labeled with blue or red color, which represents positive or negative AH sign. The zeroth Landau levels are shown in red and the other Landau levels are shown in green. (d)–(e) Illustration of two surface states with an electric field (d) $E > 0$ and (e) $E < 0$.

Anomalous Hall hysteresis loop.—For even SL MBT, there are two degenerate AFM configurations, labeled as AFM1 and AFM2 [Fig. 1(b)], related by either inversion $\hat{I}$ or time reversal symmetry $\hat{T}$. This degeneracy is lifted in the presence of both magnetic and electric fields from asymmetric substrates or electric gates [42,53]. To describe AFM configurations, we consider a two-surface-state model with the Hamiltonian $H = H_M + H_e + H_{e-M}$, where H_M describes the magnetization part, H_e is for the electron part, and H_{e-M} gives the coupling between electrons and magnetization [40,59,60]. The explicit forms of H_M, H_e, H_{e-M} are given in the Supplemental Material Sec. II.A [45]. Magnetic simulations in Refs. [13] and [40] suggest that the ground state of H_M is the out-of-plane AFM configurations, namely, AFM1 and AFM2 in Fig. 1(b) that are degenerate under H_M, at low magnetic fields B. The FM state is energetically favored at larger B.

The ground state energy for AFM1 and AFM2 can be distinguished by including electron energy of $H_e + H_{e-M}$, which involves the Landau level (LL) spectrum under B (Supplemental Material Sec. II.A [45]). For Dirac surface states, besides the normal LLs, there are additional zeroth LLs (zLLs), depicted in Fig. 1(c). All the higher LLs are equivalent for AFM1 and AFM2, and the energy difference solely comes from zLLs with the eigenenergies $\varepsilon^0_{1,\lambda} = \lambda g M_s + \lambda V_0/2$ for AFM1 and $\varepsilon^0_{2,\lambda} = \lambda g M_s - \lambda V_0/2$ for AFM2 under positive B, where $\lambda = +\,(\lambda = -)$ corresponds to zLL on the conduction band bottom (valence band top), V_0 is the asymmetric potential between two surfaces induced by electric fields, g is the exchange coupling coefficient, and M_s is the saturation magnetization. When g is positive, the zLL for the top surface state corresponds to the energy at the conduction band bottom (valence band top) for AFM1 (AFM2) while that for the bottom surface state is at the valence band top (conduction band bottom), in Fig. 1(c). At $V_0 = 0$, the occupied zLL has the same energy for two AFM configurations $\varepsilon^0_{1,-} = \varepsilon^0_{2,-} = -gM_s$. However, this degeneracy will be broken by an electric field, which shifts the zLL energies $\varepsilon^0_{1,-}$ and $\varepsilon^0_{2,-}$ oppositely. For $V_0 > 0$, the zLL energy of AFM1 decreases ($\varepsilon^0_{1,-} = -gM_s - V_0/2$) while that of AFM2 increases ($\varepsilon^0_{2,-} = -gM_s + V_0/2$) [Fig. 1(d)], and the energy difference is $\Delta\varepsilon = \varepsilon^0_{1,-} - \varepsilon^0_{2,-} = -V_0 < 0$. Therefore, AFM1 is energetically favored for $V_0 > 0$, corresponding to parallel alignment of electric and magnetic fields $\boldsymbol{B}\cdot\boldsymbol{E} > 0$ (we choose $V_0 = eEL$ with E representing electric field and L the film thickness). For $V_0 < 0$ ($\boldsymbol{B}\cdot\boldsymbol{E} < 0$), AFM2 has a lower ground state energy ($\Delta\varepsilon = -V_0 > 0$). Therefore, the energy difference between two AFM states microscopically arises from the energy shift of zLLs under electric fields.

After identifying the lower-energy AFM configurations under magnetic and electric fields, we next study the sign of AH conductance. To be consistent with negative AH sign for odd SLs in Ref. [44], exchange coupling g should be positive, so that the valence bands of both surface states in odd SLs contribute negative AH sign (Supplemental Material Sec. III [45]). For even SLs, the AH signs are reversed for the surface whose magnetization is flipped compared to that of odd SLs; for Fermi energy inside magnetic gap, the valence bands of top and bottom surfaces give exact opposite contributions, leading to zero overall AH conductance, as shown in Fig. 1(c), where blue and red colors stand for positive and negative AH signs, respectively. For the system with $B > 0$ and $E > 0$ ($V_0 > 0$) at electron doping, the favored AFM configuration is AFM1 with a positive AH conductance at electron doping [Fig. 1(d)]. When $E < 0$ ($V_0 < 0$), the favored AFM configuration is AFM2, also exhibiting positive AH conductance at electron doping [Fig. 1(e)]. With similar analysis for $B < 0$, we conclude that the odd and even SL films will always have opposite AH signs at electron doping, independent of the alignment between E and B. These results explain the observations of the even-odd AH effect in the samples with electron doping.

To buttress our arguments, we also investigate a thin film model which includes both surface and bulk states, and perform numerical calculations for the zLL energies and the AH conductivity for 2-SL MBT in Fig. 2 (Supplemental Material Sec. II.B [45]). For $\boldsymbol{B}\cdot\boldsymbol{E} > 0$, $\Delta\varepsilon = \varepsilon_{\mathrm{AFM1}} - \varepsilon_{\mathrm{AFM2}} < 0$ so that AFM1 is energetically favored, while for $\boldsymbol{B}\cdot\boldsymbol{E} < 0$, AFM2 is preferred [Fig. 2(b)]. We then

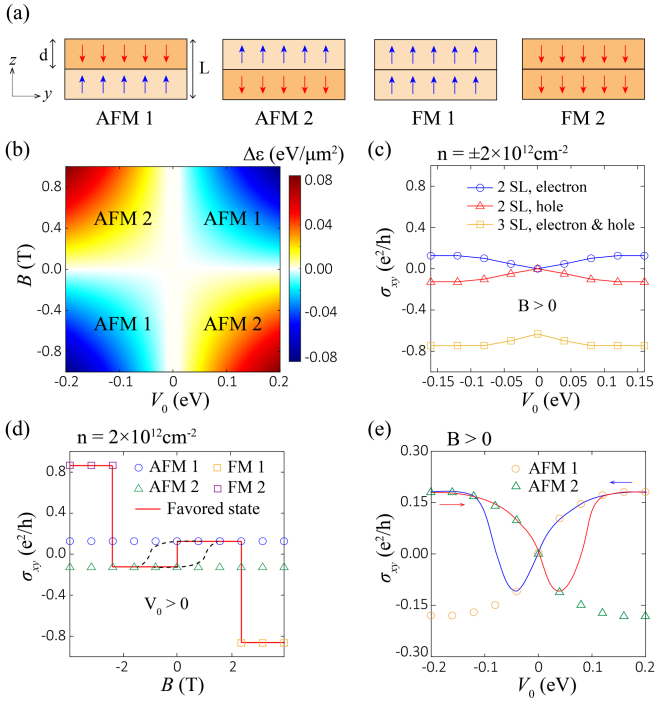

FIG. 2. (a) Illustration of thin film model for 2 SL MBT films. Each SL has a thickness of d. (b) The energy density difference between AFM1 and AFM2 $\Delta\varepsilon = \varepsilon_1 - \varepsilon_2$ as a function of asymmetric potential V_0 and magnetic field B at electron density $n = 2 \times 10^{12}$ cm^{-2}. (c) Numerically calculated Hall conductance σ_{xy} as a function of V_0 for favored 2 SL and 3 SL samples at electron and hole doping under positive B with carrier density $n = \pm 2 \times 10^{12}$ cm^{-2}. (d) Hall conductance σ_{xy} as a function of B at electron density $n = 2 \times 10^{12}$ cm^{-2} for positive V_0. The red line is the expected favored state at different B. The dashed black lines illustrate the hysteresis loop. (e) Electric control of Hall conductivity for 2 SL. The yellow circles and green triangles stand for the Hall conductivity for AFM1 and AFM2, respectively. The solid lines of sweeping V_0 are sketched by hand only for illustration.

compare the Hall conductivity in 2-SL and 3-SL MBT at both electron and hole doping with carrier density $n = \pm 2 \times 10^{-12}$ cm^{-2} for positive B in Fig. 2(c). A nonzero V_0 can induce a positive (negative) AH response in 2-SL MBT at electron doping (hole doping). For 3-SL MBT, the AH sign does not change with doping or electric fields. In summary, the 2-SL and 3-SL MBT show opposite AH signs at electron doping, while they have the same AH sign at hole doping, consistent with the analysis of the two-surface-state model. This prediction is in agreement with the experiment in Ref. [53], and the resulting AH sign is also consistent with the previously proposed even-odd effect in the insulating regime [11–13] (Supplemental Material Sec. III [45]).

We further investigate the hysteresis loop for even SL MBT. Figure 2(d) shows the Hall conductivity σ_{xy} for both the AFM and FM states at electron density $n = 2 \times 10^{-12}$ cm^{-2} for $V_0 > 0$ and sketch the expected favored states at different B by red line. The spin-flop transition field B_c for 2-MBT film is around 2.3 T in experiment [44]. For $|B| > B_c$, the FM states have the lower magnetization energy and thus are energetically favored. For $|B| < B_c$, the AFM states have lower energy, and AFM1 is favored at $0 < B < B_c$, while AFM2 is preferred at $-B_c < B < 0$ for $V_0 > 0$. When the magnetic field is swept from positive to negative, the favored state for 2-SL films goes through FM1 $\rightarrow$ AFM1 $\rightarrow$ AFM2 $\rightarrow$ FM2 and, correspondingly, the sign of Hall conductivity σ_{xy} varies as $- \rightarrow + \rightarrow - \rightarrow +$ [the red lines in Fig. 2(d)]. Since the AFM1-AFM2 phase transition is of first order, a hysteresis loop can form at small B before spin-flop transition [the black dashed lines in Fig. 2(d)], corresponding to the observed AH hysteresis loop in Fig. 1(a). Thus, the double sign changes of the hysteresis loop can be naturally understood as a two-step phase transition: the first-step transition between two AFM states followed by the second-step transition between the AFM and FM states. For even SL MBT films thicker than 2 SL, multistep spin-flop phase transitions might occur due to multiple FM configurations [41] (Supplemental Material Sec. IV [45]).

The dependence of AFM ground state energy on electric fields implies the possibility of electrical control of AH conductance near AFM transition. If we sweep electric fields from positive to negative [the blue curve in Fig. 2(e)], the favored configuration changes from AFM1 to AFM2 according to Fig. 2(b), and, correspondingly, Hall conductivity first changes from positive to negative momentarily then back to positive due to hysteresis. This electric control of AH conductance potentially provides a microscopic picture to understand recent experiments [53].

Orbital magnetization and magnetoelectric effect.—Next we will discuss an alternative view point of AFM transition based on orbital magnetization created by the magnetoelectric effect in MBT films. In magnetic materials, spin moment is usually much larger than orbital moment. The odd-SL MBT has an uncompensated net spin magnetization, and thus orbital magnetization is negligible. For even SLs, however, spin magnetization cancels out in AFM configurations, and orbital magnetization can play a role. The orbital magnetization in even SL MBT can lead to the magnetoelectric effect, e.g., an electric field can create a magnetization, given by $\mathbf{M} = \alpha \mathbf{E}$, with magnetoelectric coefficient α. The magnetoelectric effect has been previously studied in 2D magnetic materials [61,62].

Orbital magnetization usually contains two parts, a trivial and a topological part, $\boldsymbol{m}_{\text{total}} = \boldsymbol{m}_{\text{trivial}} + \boldsymbol{m}_{\text{topo}}$ [63–66]. Figures 3(a)–3(d) show orbital magnetic moments as a function of V_0 for 2-5 SLs in a thin film model at $\mu = 0$ (Supplemental Material Sec. VII [45]). For odd SLs [Figs. 3(b) and 3(d)], the orbital moment remains constant, while for even SLs [Figs. 3(a) and 3(c)], the orbital moment is zero at $V_0 = 0$ and linearly increases with V_0 for AFM1.

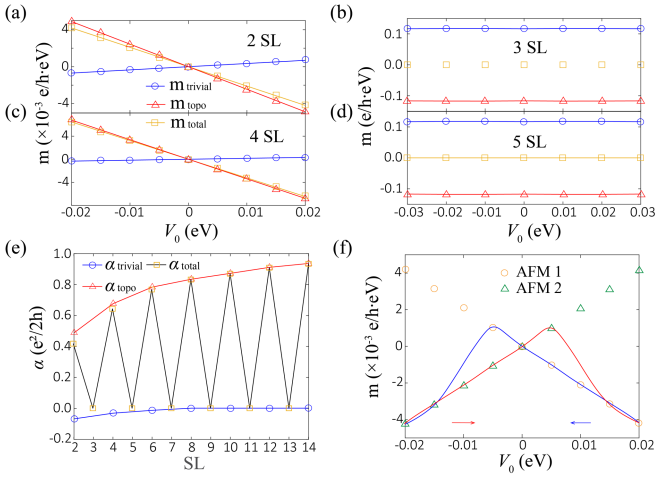

FIG. 3. Calculated orbital magnetic moment m as a function of V_0 for (a) 2SL, (b) 3SL, (c) 4SL, and (d) 5SL in the thin film model for chemical potential $\mu = 0$. The blue, red, and yellow lines are for trivial, topological, and total magnetic moment, respectively. (e) The trivial and topological part of α and total α as a function of SL number. (f) Illustration of the electric control of orbital magnetic moment in even SL MBT.

This linear behavior implies the magnetoelectric effect in even SL MBT. The signs of magnetic moments reverse for AFM2. With magnetic fields, the electric-field-induced orbital magnetization can lead to the energy difference $\Delta\varepsilon = \varepsilon_{\mathrm{AFM1}} - \varepsilon_{\mathrm{AFM2}} = \boldsymbol{M}_{\mathrm{orb},1} \cdot \boldsymbol{B} - \boldsymbol{M}_{\mathrm{orb},2} \cdot \boldsymbol{B}$ between two AFM states, where $\boldsymbol{M}_{\mathrm{orb},1}$ and $\boldsymbol{M}_{\mathrm{orb},2}$ are orbital magnetization of AFM1 and AFM2, respectively. A positive electric field, namely, $V_0 > 0$, can induce a negative (positive) total orbital magnetization $\boldsymbol{M}_{\mathrm{orb},1} = -M_0\hat{z}$ ($\boldsymbol{M}_{\mathrm{orb},2} = M_0\hat{z}$) for the AFM1 (AFM2) configuration, where M_0 is a positive number and $\hat{z}$ is the unit vector along the z axis, so $\Delta\varepsilon = -2M_0B < 0$ at positive B, which means AFM1 is favored, and $\Delta\varepsilon = 2M_0B > 0$ at $-B$, for which AFM2 is favored. The above analysis is quantitatively consistent with the perspective of zLLs (Supplemental Material Sec. VII [45]).

For an electric field strength $E \approx 0.1$ V/nm, orbital moments in even SL MBT is estimated as $10^{-1}(e/h) \cdot \mathrm{eV} \sim 0.4\ \mu_B/\mathrm{nm}^2$ with $(e/h) \simeq 4.18\ \mu_B/(\mathrm{nm}^2 \cdot \mathrm{eV})$ and Bohr magneton $\mu_B = (e\hbar/2m_e)$. With the magnetic moment $\sim 5\mu_B$ of Mn ions and the in-plane lattice constant $a \simeq 0.43$ nm of MBT [2], spin magnetization is around $27\ \mu_B/\mathrm{nm}^2$, and hence orbital magnetization is approximately 2 orders smaller than spin magnetization, which thus can only play a role in compensated AFM configuration.

We can further extract the magnetoelectric coefficient α from orbital magnetization [67–69]. In Fig. 3(e), the trivial part of α goes to zero and the topological part approaches quantized value $e^2/2h$ as the layer number increases for even SLs at $\mu = 0$ [37,59]. The odd SLs always exhibit zero α with a constant orbital magnetization. Thus, α oscillates between zero and nonzero for odd and even SLs of MBT films [Fig. 3(e)]. The behaviors of α for a nonzero chemical potential μ are discussed in Supplemental Material Sec. VII [45].

We should distinguish magnetoelectric coefficient α from the axion parameter θ, a three-dimensional (3D) bulk quantity that characterizes the axion term $\theta e^2\mathbf{E} \cdot \mathbf{B}/2\pi h$ in electromagnetic response of topological insulators [13,35,67–71]. θ can be directly connected to magnetoelectric coefficient α (an experimental observable) as $\alpha = \theta e^2/2\pi h$ when all the surface states of 3D TIs are gapped. For the MBT films, this corresponds to even SLs in the large thickness limit, and the magnetoelectric coefficient α value approaches $e^2/2h$ [Fig. 3(e)] as $\theta = \pi$ in bulk MBT. For the thick odd-SL MBT, the magnetoelectric coefficient α is zero, different from the bulk axion parameter $\theta = \pi$. Because of $\theta = \pi$, such phase was previously referred to as AIs with higher-order topology [14,23,24,34,72–74]. In Supplemental Material Sec. VII [45], we show while the total orbital magnetization depends on bulk magnetic configurations, the magnetoelectric coefficient α only depends on the surface magnetization, insensitive to bulk magnetization.

Orbital magnetization in even SL MBT can have an impact in magnetic circular dichroism (MCD) [43]. Early RMCD experiments in even SLs show a nonzero hysteresis loop around small magnetic fields [40,41]. Our studies of orbital magnetization provide an intrinsic mechanism for these observations. A decent RMCD signal may also come from the p-d transition of magnetic ions, or the difference in the reflections between two surface states [75]. MCD signals of orbital magnetization in even SLs can also be controlled by sweeping electric fields. Following the blue curve in Fig. 3(f), AFM1 is the favored configuration with negative orbital magnetization at positive V_0, and magnetization vanishes at $V_0 = 0$. As V_0 turns to negative, the system remains in the AFM1 with positive orbital magnetization as the AFM1-AFM2 transition is of first order, giving rise to a hysteresis loop, similar to the AH hysteresis loop discussed in Fig. 2(e). Therefore, orbital magnetization is expected to vary from negative to positive then back to negative as the electric potential V_0 sweeps from positive to negative.

Conclusion.—In summary, we apply a two-surface-state model and a thin-film model to MBT films, and demonstrate that the presence of electric and magnetic fields can select a favored AFM configuration in even SLs through the effect of zLLs, leading to a nonzero AH response and orbital magnetization. For real samples, disorders and magnetic domains are inevitable (Supplemental Material Sec. VI [45]). For example, antiferromagnetic domain walls have been imaged in MBT via cryogenic magnetic force microscopy [76]. Thus, the AFM transition should correspond to enlargement and shrinkage of two opposite AFM domains. Furthermore, bulk states, in addition to surface states, may also play a role due to chemical potential inhomogeneity, potentially leading to more complicated

behaviors [54]. More experimental studies are necessary to validate our prediction of the AH effect in even and odd SL MBT at electron and hole dopings, as well as the possible electric control of orbital magnetization in even SL MBT.

We would like to acknowledge Binghai Yan for the helpful discussion. R. B. M. and C.-X. L. acknowledge the support through the Penn State MRSEC-Center for Nanoscale Science via NSF Grant No. DMR-2011839. C.-X. L. also acknowledges the support of NSF Grant No. (DMR-2241327). Y.-F. Z. and C.-Z. C. acknowledge the support from the ARO Grant (W911NF2210159) and the Gordon and Betty Moore Foundation's EPiQS Initiative (Grant No. GBMF9063 to C.-Z. C.). D. X. is supported by AFOSR MURI 2D MAGIC (FA9550-19-1-0390).

[1] M. M. Otrokov, T. V. Menshchikova, M. G. Vergniory, I. P. Rusinov, A. Y. Vyazovskaya, Y. M. Koroteev, G. Bihlmayer, A. Ernst, P. M. Echenique, A. Arnau *et al.*, Highly-ordered wide bandgap materials for quantized anomalous Hall and magnetoelectric effects, 2D Mater. **4**, 025082 (2017).

[2] J.-Q. Yan, Q. Zhang, T. Heitmann, Z. Huang, K. Y. Chen, J.-G. Cheng, W. Wu, D. Vaknin, B. C. Sales, and R. J. McQueeney, Crystal growth and magnetic structure of $MnBi_2Te_4$, Phys. Rev. Mater. **3**, 064202 (2019).

[3] Y. Gong *et al.*, Experimental realization of an intrinsic magnetic topological insulator, Chin. Phys. Lett. **36**, 076801 (2019).

[4] M. M. Otrokov, I. I. Klimovskikh, H. Bentmann, D. Estyunin, A. Zeugner, Z. S. Aliev, S. Gaß, A. Wolter, A. Koroleva, A. M. Shikin *et al.*, Prediction and observation of an antiferromagnetic topological insulator, Nature (London) **576**, 416 (2019).

[5] J. Wu, F. Liu, M. Sasase, K. Ienaga, Y. Obata, R. Yukawa, K. Horiba, H. Kumigashira, S. Okuma, T. Inoshita *et al.*, Natural van der Waals heterostructural single crystals with both magnetic and topological properties, Sci. Adv. **5**, eaax9989 (2019).

[6] M. Shi, B. Lei, C. Zhu, D. Ma, J. Cui, Z. Sun, J. Ying, and X. Chen, Magneticand transport properties in the magnetic topological insulators $MnBi_2Te_4(Bi_2Te_3)_n$ $(n = 1, 2)$, Phys. Rev. B **100**, 155144 (2019).

[7] K. He, $MnBi_2Te_4$-family intrinsic magnetic topological materials, npj Quantum Mater. **5**, 90 (2020).

[8] J. Liu and T. Hesjedal, Magnetic topological insulator heterostructures: A review, Adv. Mater. **35**, 2102427 (2021).

[9] C.-Z. Chang, Marriage of topology and magnetism, Nat. Mater. **19**, 484 (2020).

[10] C.-Z. Chang, C.-X. Liu, and A. H. MacDonald, Colloquium: Quantum anomalous Hall effect, Rev. Mod. Phys. **95**, 011002 (2023).

[11] M. M. Otrokov, I. P. Rusinov, M. Blanco-Rey, M. Hoffmann, A. Y. Vyazovskaya, S. V. Eremeev, A. Ernst, P. M. Echenique, A. Arnau, and E. V. Chulkov, Unique thickness-dependent properties of the van der Waals interlayer antiferromagnet $MnBi_2Te_4$ films, Phys. Rev. Lett. **122**, 107202 (2019).

[12] J. Li, Y. Li, S. Du, Z. Wang, B.-L. Gu, S.-C. Zhang, K. He, W. Duan, and Y. Xu, Intrinsic magnetic topological insulators in van der Waals layered $MnBi_2Te_4$-family materials, Sci. Adv. **5**, eaaw5685 (2019).

[13] D. Zhang, M. Shi, T. Zhu, D. Xing, H. Zhang, and J. Wang, Topological axion states in the magnetic insulator $MnBi_2Te_4$ with the quantized magnetoelectric effect, Phys. Rev. Lett. **122**, 206401 (2019).

[14] R.-X. Zhang, F. Wu, and S. Das Sarma, Möbius insulator and higher-order topology in $MnBi_{2n}Te_{3n+1}$, Phys. Rev. Lett. **124**, 136407 (2020).

[15] Y. J. Chen *et al.*, Topological electronic structure and its temperature evolution in antiferromagnetic topological insulator $MnBi_2Te_4$, Phys. Rev. X **9**, 041040 (2019).

[16] D. Estyunin, I. I. Klimovskikh, A. M. Shikin, E. Schwier, M. Otrokov, A. Kimura, S. Kumar, S. Filnov, Z. S. Aliev, M. Babanly *et al.*, Signatures of temperature driven antiferromagnetic transition in the electronic structure of topological insulator $MnBi_2Te_4$, APL Mater. **8**, 021105 (2020).

[17] D. Nevola, H. X. Li, J.-Q. Yan, R. Moore, H.-N. Lee, H. Miao, and P. D. Johnson, Coexistence of surface ferromagnetism and a gapless topological state in $MnBi_2Te_4$, Phys. Rev. Lett. **125**, 117205 (2020).

[18] C. Yan, S. Fernandez-Mulligan, R. Mei, S. H. Lee, N. Protic, R. Fukumori, B. Yan, C. Liu, Z. Mao, and S. Yang, Origins of electronic bands in the antiferromagnetic topological insulator $MnBi_2Te_4$, Phys. Rev. B **104**, L041102 (2021).

[19] E. D. Rienks, S. Wimmer, J. Sánchez-Barriga, O. Caha, P. S. Mandal, J. Růžička, A. Ney, H. Steiner, V. V. Volobuev, H. Groiß *et al.*, Large magnetic gap at the Dirac point in $Bi_2Te_3/MnBi_2Te_4$ heterostructures, Nature (London) **576**, 423 (2019).

[20] P. Swatek, Y. Wu, L.-L. Wang, K. Lee, B. Schrunk, J. Yan, and A. Kaminski, Gapless Dirac surface states in the antiferromagnetic topological insulator $MnBi_2Te_4$, Phys. Rev. B **101**, 161109 (2020).

[21] X.-L. Qi and S.-C. Zhang, Topological insulators and superconductors, Rev. Mod. Phys. **83**, 1057 (2011).

[22] D. Xiao, J. Jiang, J.-H. Shin, W. Wang, F. Wang, Y.-F. Zhao, C. Liu, W. Wu, M. H. W. Chan, N. Samarth, and C. Z. Chang, Realization of the axion insulator state in quantum anomalous Hall sandwich heterostructures, Phys. Rev. Lett. **120**, 056801 (2018).

[23] Y. Xu, Z. Song, Z. Wang, H. Weng, and X. Dai, Higher-order topology of the axion insulator $EuIn_2As_2$, Phys. Rev. Lett. **122**, 256402 (2019).

[24] R. Chen, S. Li, H.-P. Sun, Q. Liu, Y. Zhao, H.-Z. Lu, and X. Xie, Using nonlocal surface transport to identify the axion insulator, Phys. Rev. B **103**, L241409 (2021).

[25] M. Gu, J. Li, H. Sun, Y. Zhao, C. Liu, J. Liu, H. Lu, and Q. Liu, Spectral signatures of the surface anomalous Hall effect in magnetic axion insulators, Nat. Commun. **12**, 3524 (2021).

[26] C. Liu, Y. Wang, H. Li, Y. Wu, Y. Li, J. Li, K. He, Y. Xu, J. Zhang, and Y. Wang, Robust axion insulator and Chern insulator phases in a two-dimensional antiferromagnetic topological insulator, Nat. Mater. **19**, 522 (2020).

[27] M. Mogi, M. Kawamura, R. Yoshimi, A. Tsukazaki, Y. Kozuka, N. Shirakawa, K. Takahashi, M. Kawasaki, and Y. Tokura, A magnetic heterostructure of topological insulators as a candidate for an axion insulator, Nat. Mater. **16**, 516 (2017).

[28] M. Mogi, M. Kawamura, A. Tsukazaki, R. Yoshimi, K. S. Takahashi, M. Kawasaki, and Y. Tokura, Tailoring tricolor structure of magnetic topological insulator for robust axion insulator, Sci. Adv. **3**, eaao1669 (2017).

[29] H. Li, H. Jiang, C.-Z. Chen, and X. C. Xie, Critical behavior and universal signature of an axion insulator state, Phys. Rev. Lett. **126**, 156601 (2021).

[30] Z.-D. Song, B. Lian, R. Queiroz, R. Ilan, B. A. Bernevig, and A. Stern, Delocalization transition of a disordered axion insulator, Phys. Rev. Lett. **127**, 016602 (2021).

[31] K. M. Fijalkowski, N. Liu, M. Hartl, M. Winnerlein, P. Mandal, A. Coschizza, A. Fothergill, S. Grauer, S. Schreyeck, K. Brunner, M. Greiter, R. Thomale, C. Gould, and L. W. Molenkamp, Any axion insulator must be a bulk three-dimensional topological insulator, Phys. Rev. B **103**, 235111 (2021).

[32] G. M. Pierantozzi, A. De Vita, C. Bigi, X. Gui, H.-J. Tien, D. Mondal, F. Mazzola, J. Fujii, I. Vobornik, G. Vinai *et al.*, Evidence of magnetism-induced topological protection in the axion insulator candidate $EuSn_2P_2$, Proc. Natl. Acad. Sci. U.S.A. **119**, e2116575119 (2022).

[33] J. Yu, J. Zang, and C.-X. Liu, Magnetic resonance induced pseudoelectric field and giant current response in axion insulators, Phys. Rev. B **100**, 075303 (2019).

[34] C. Yue, Y. Xu, Z. Song, H. Weng, Y.-M. Lu, C. Fang, and X. Dai, Symmetry-enforced chiral hinge states and surface quantum anomalous Hall effect in the magnetic axion insulator $Bi_{2-x}Sm_xSe_3$, Nat. Phys. **15**, 577 (2019).

[35] A. Sekine and K. Nomura, Axion electrodynamics in topological materials, J. Appl. Phys. **129**, 141101 (2021).

[36] R. Li, J. Wang, X.-L. Qi, and S.-C. Zhang, Dynamical axion field in topological magnetic insulators, Nat. Phys. **6**, 284 (2010).

[37] R. Chen, H.-P. Sun, and B. Zhou, Side-surface-mediated hybridization in axion insulators, Phys. Rev. B **107**, 125304 (2023).

[38] B. Chen *et al.*, Intrinsic magnetic topological insulator phases in the Sb doped $MnBi_2Te_4$ bulks and thin flakes, Nat. Commun. **10**, 4469 (2019).

[39] Y. Deng, Y. Yu, M. Z. Shi, Z. Guo, Z. Xu, J. Wang, X. H. Chen, and Y. Zhang, Quantum anomalous Hall effect in intrinsic magnetic topological insulator $MnBi_2Te_4$, Science **367**, 895 (2020).

[40] D. Ovchinnikov, X. Huang, Z. Lin, Z. Fei, J. Cai, T. Song, M. He, Q. Jiang, C. Wang, H. Li, Y. Wang, Y. Wu, D. Xiao, J.-H. Chu, J. Yan, C.-Z. Chang, Y.-T. Cui, and X. Xu, Intertwined topological and magnetic orders in atomically thin chern insulator $MnBi_2Te_4$, Nano Lett. **21**, 2544 (2021).

[41] S. Yang, X. Xu, Y. Zhu, R. Niu, C. Xu, Y. Peng, X. Cheng, X. Jia, Y. Huang, X. Xu *et al.*, Odd-even layer-number effect and layer-dependent magnetic phase diagrams in $MnBi_2Te_4$, Phys. Rev. X **11**, 011003 (2021).

[42] J. Cai, D. Ovchinnikov, Z. Fei, M. He, T. Song, Z. Lin, C. Wang, D. Cobden, J.-H. Chu, Y.-T. Cui *et al.*, Electric control of a canted-antiferromagnetic chern insulator, Nat. Commun. **13**, 1668 (2022).

[43] J.-X. Qiu, C. Tzschaschel, J. Ahn, A. Gao, H. Li, X.-Y. Zhang, B. Ghosh, C. Hu, Y.-X. Wang, Y.-F. Liu *et al.*, Axion optical induction of antiferromagnetic order, Nat. Mater. **22**, 583 (2023).

[44] Y.-F. Zhao, L.-J. Zhou, F. Wang, G. Wang, T. Song, D. Ovchinnikov, H. Yi, R. Mei, K. Wang, M. H. W. Chan, C.-X. Liu, X. Xu, and C.-Z. Chang, Even–odd layer-dependent anomalous Hall effect in topological magnet $MnBi_2Te_4$ thin films, Nano Lett. **21**, 7691 (2021).

[45] See Supplemental Material at http://link.aps.org/supplemental/10.1103/PhysRevLett.132.066604 for details of experimental observations, model Hamiltonian, disorder effect, and orbital magnetization, which includes Refs. [46–52].

[46] E. Novik, A. Pfeuffer-Jeschke, T. Jungwirth, V. Latussek, C. R. Becker, G. Landwehr, H. Buhmann, and L. W. Molenkamp, Band structure of semimagnetic $Hg_{1-y}Mn_yTe$ quantum wells, Phys. Rev. B **72**, 035321 (2005).

[47] C.-X. Liu, X.-L. Qi, H. J. Zhang, X. Dai, Z. Fang, and S.-C. Zhang, Model Hamiltonian for topological insulators, Phys. Rev. B **82**, 045122 (2010).

[48] P. M. Sass, J. Kim, D. Vanderbilt, J. Yan, and W. Wu, Robust A-type order and spin-flop transition on the surface of the antiferromagnetic topological insulator $MnBi_2Te_4$, Phys. Rev. Lett. **125**, 037201 (2020).

[49] S.-K. Bac, K. Koller, F. Lux, J. Wang, L. Riney, K. Borisiak, W. Powers, M. Zhukovskyi, T. Orlova, M. Dobrowolska *et al.*, Topological response of the anomalous Hall effect in $MnBi_2Te_4$ due to magnetic canting, npj Quantum Mater. **7**, 46 (2022).

[50] S. Onoda, N. Sugimoto, and N. Nagaosa, Intrinsic versus extrinsic anomalous Hall effect in ferromagnets, Phys. Rev. Lett. **97**, 126602 (2006).

[51] N. Nagaosa, J. Sinova, S. Onoda, A. H. MacDonald, and N. P. Ong, Anomalous Hall effect, Rev. Mod. Phys. **82**, 1539 (2010).

[52] D. Xiao, W. Yao, and Q. Niu, Valley-contrasting physics in graphene: Magnetic moment and topological transport, Phys. Rev. Lett. **99**, 236809 (2007).

[53] A. Gao *et al.*, Layer Hall effect in a 2D topological axion antiferromagnet, Nature (London) **595**, 521 (2021).

[54] S. Zhang, R. Wang, X. Wang, B. Wei, B. Chen, H. Wang, G. Shi, F. Wang, B. Jia, Y. Ouyang, F. Xie, F. Fei, M. Zhang, X. Wang, D. Wu, X. Wan, F. Song, H. Zhang, and B. Wang, Experimental observation of the gate-controlled reversal of the anomalous Hall effect in the intrinsic magnetic topological insulator $MnBi_2Te_4$ device, Nano Lett. **20**, 709 (2020).

[55] D. J. Huang, C. F. Chang, H.-T. Jeng, G. Y. Guo, H.-J. Lin, W. B. Wu, H. C. Ku, A. Fujimori, Y. Takahashi, and C. T. Chen, Spin and orbital magnetic moments of Fe_3O_4, Phys. Rev. Lett. **93**, 077204 (2004).

[56] X. Lu, P. Stepanov, W. Yang, M. Xie, M. A. Aamir, I. Das, C. Urgell, K. Watanabe, T. Taniguchi, G. Zhang *et al.*, Superconductors, orbital magnets and correlated states in magic-angle bilayer graphene, Nature (London) **574**, 653 (2019).

[57] A. L. Sharpe, E. J. Fox, A. W. Barnard, J. Finney, K. Watanabe, T. Taniguchi, M. Kastner, and D. Goldhaber-Gordon, Emergent ferromagnetism near three-quarters filling in twisted bilayer graphene, Science **365**, 605 (2019).
[58] W.-Y. He, D. Goldhaber-Gordon, and K. T. Law, Giant orbital magnetoelectric effect and current-induced magnetization switching in twisted bilayer graphene, Nat. Commun. **11**, 1650 (2020).
[59] Y.-H. Li and R. Cheng, Identifying axion insulator by quantized magnetoelectric effect in antiferromagnetic $MnBi_2Te_4$ tunnel junction, Phys. Rev. Res. **4**, L022067 (2022).
[60] D. Mills and W. Saslow, Surface effects in the Heisenberg antiferromagnet, Phys. Rev. **171**, 488 (1968).
[61] Y. Lu, R. Fei, X. Lu, L. Zhu, L. Wang, and L. Yang, Artificial multiferroics and enhanced magnetoelectric effect in van der Waals heterostructures, ACS Appl. Mater. Interfaces **12**, 6243 (2020).
[62] J. Shang, X. Tang, Y. Gu, A. V. Krasheninnikov, S. Picozzi, C. Chen, and L. Kou, Robust magnetoelectric effect in the decorated graphene/In_2Se_3 heterostructure, ACS Appl. Mater. Interfaces **13**, 3033 (2021).
[63] D. Xiao, J. Shi, and Q. Niu, Berry phase correction to electron density of states in solids, Phys. Rev. Lett. **95**, 137204 (2005).
[64] I. Souza and D. Vanderbilt, Dichroic f-sum rule and the orbital magnetization of crystals, Phys. Rev. B **77**, 054438 (2008).
[65] D. Xiao, M.-C. Chang, and Q. Niu, Berry phase effects on electronic properties, Rev. Mod. Phys. **82**, 1959 (2010).
[66] T. Thonhauser, Theory of orbital magnetization in solids, Int. J. Mod. Phys. B **25**, 1429 (2011).
[67] A. M. Essin, J. E. Moore, and D. Vanderbilt, Magnetoelectric polarizability and axion electrodynamics in crystalline insulators, Phys. Rev. Lett. **102**, 146805 (2009).
[68] A. M. Essin, A. M. Turner, J. E. Moore, and D. Vanderbilt, Orbital magnetoelectric coupling in band insulators, Phys. Rev. B **81**, 205104 (2010).
[69] J. Wang, B. Lian, X.-L. Qi, and S.-C. Zhang, Quantized topological magnetoelectric effect of the zero-plateau quantum anomalous Hall state, Phys. Rev. B **92**, 081107(R) (2015).
[70] F. Wilczek, Two applications of axion electrodynamics, Phys. Rev. Lett. **58**, 1799 (1987).
[71] X.-L. Qi, T. L. Hughes, and S.-C. Zhang, Topological field theory of time-reversal invariant insulators, Phys. Rev. B **78**, 195424 (2008).
[72] B. J. Wieder and B. A. Bernevig, The axion insulator as a pump of fragile topology, arXiv:1810.02373.
[73] N. Varnava and D. Vanderbilt, Surfaces of axion insulators, Phys. Rev. B **98**, 245117 (2018).
[74] N. Varnava, J. H. Wilson, J. Pixley, and D. Vanderbilt, Controllable quantum point junction on the surface of an antiferromagnetic topological insulator, Nat. Commun. **12**, 3998 (2021).
[75] J. Ahn, S.-Y. Xu, and A. Vishwanath, Theory of optical axion electrodynamics and application to the Kerr effect in topological antiferromagnets, Nat. Commun. **13**, 7615 (2022).
[76] P. M. Sass, W. Ge, J. Yan, D. Obeysekera, J. Yang, and W. Wu, Magnetic imaging of domain walls in the antiferromagnetic topological insulator $MnBi_2Te_4$, Nano Lett. **20**, 2609 (2020).